World Conference on Timber Engineering Oslo 2023

DEVELOPMENT OF HYBRID RIGID FRAME STRUCTURE METHOD USING SEMI-RIGID TIMBER BEAMS

Akihiko Miyake,[1] Ryoma Murata[2]

ABSTRACT: The authors are working to develop a construction method that incorporates semi-rigid timber beams into a steel frame structure to form a rigid frame structure. In structures constructed by this method, the joints of the semi-rigid timber beams, consisting of drift pins inserted into steel plates, resist seismic moments, generating a bending yield at the root end of the inserted U-shaped steel plates. We believe this explains the specified bearing strength and deformability achieved. We performed experiments and analysis to verify the structural performance of structures incorporating CLT semi-rigid beams. This paper describes the results of full-size in-plane bending tests performed on semi-rigid beam joints; tensile tests performed on individual drift pin joints; and the finite element method analysis used to assess the experimental results.

KEY WORDS: Medium- and large-scale timber building, hybrid structure, CLT, semi-rigid beam, inserted steel plate and drift pin joints

1 INTRODUCTION

There has been growing interest in recent years in using timber—particularly for medium- and large-scale buildings—to promote a low-carbon society and to make more effective use of domestic forestry resources. In Japan, growing numbers of medium- and high-rise buildings feature timber construction or hybrid construction incorporating timber.

This study discusses the development of a rigid frame construction method that incorporates timber beams into a steel structure (Figure 1).

This method involves connecting semi-rigid timber beams to steel columns. The inserted steel plate and drift pin joints at the ends of the beams function as rigid frame beams and resist lateral forces during an earthquake. The timber beams bear the bending moments and shear forces generated by an earthquake, while the steel beam located nearby bears the vertical loads associated with the slabs and interior and exterior materials, so that the timber beams are not subject to constant loading.

Figure 2 shows the joint. Cross laminated timber (CLT) is used for the semi-rigid timber beams. Slits are cut into the center, into which U-shaped steel plates are inserted, allowing joints using drift pins. The steel columns have brackets welded to them. Friction joints incorporating high-strength bolts between the brackets and attached plates allow the transmission of bending moments and shear forces during an earthquake. In the event of a major earthquake, it is expected that both the drift pin joints and the roots of the U-shaped steel plates will yield, ensuring deformability.

As part of this study, we performed full-size in-plane bending tests on the end of a semi-rigid beam removed from a joint between a semi-rigid timber beam and a steel column. We also performed tensile tests of individual drift pin joints to determine their characteristic values and assessed the results via finite element method analysis. This paper presents the test results, comparisons of the test results and analytical modeling results.

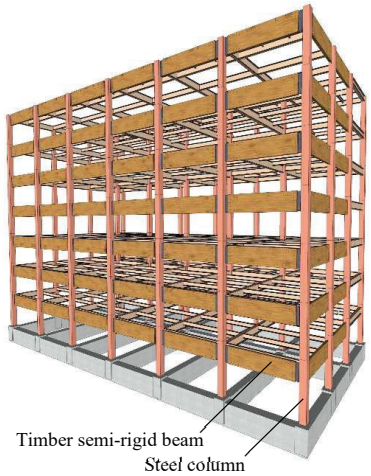

Figure 1: *Three-dimensional view of the construction*

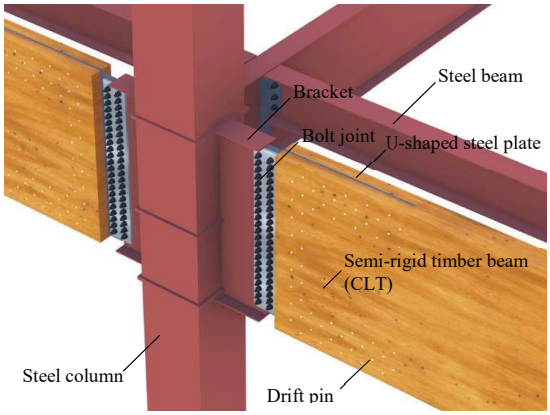

Figure 2: *Outline of the joint*

[1] Akihiko Miyake, Kumagai Gumi Co.,Ltd., Japan, akihiko.miyake@ku.kumagaigumi.co.jp

[2] Ryoma Murata, The University of Tokyo, Japan, murata@murataryoma.com

https://doi.org/10.52202/069179-0433

2 BEAM END JOINT FULL-SIZE IN-PLANE BENDING TEST

2.1 TEST AIMS

To confirm the behavior, load deformation relationship, and failure characteristics of a joint at the end of a semi-rigid timber beam subject to lateral forces during an earthquake, we extracted the section of a semi-rigid timber beam from the end to the center of the span. We then performed in-plane bending tests of the joint by repeatedly applying alternating positive and negative loads.

2.2 TEST PIECE OVERVIEW

Figure 3 shows the test piece. The CLT used for the test piece was S60-5-7 (in JAS) Japanese cedar (with the joints of the two outer-layer side-by-side plies shifted by half). One test piece was cut from each of the three parent boards. Table 1 gives the specifications for the CLT used in the tests. The test pieces here are referred to as "Cn-F," with the "n" indicating parent board number 1, 2, or 3. The inserted steel plate was made of SN400B (in JIS G3136, yield strength from 235 to 355 N/mm^2 and tensile strength from 400 to 510 N/mm^2) machined into a U-shape. The drift pins were made of SNR400B (in JIS G3138, yield strength from 215 to 335 N/mm^2 and tensile strength from 400 to 510 N/mm^2), with 55 pins arranged as shown in Figure 3. Table 2 gives the mechanical properties of the drift pins and the inserted steel plate. The holes in the CLT have a clearance of 0 mm with respect to the 16 mm diameter drift pins; the holes in the inserted steel plate have a clearance of + 1 mm; and the slit in the CLT has a clearance of + 2 mm with respect to the 19 mm thickness of the inserted steel plate.

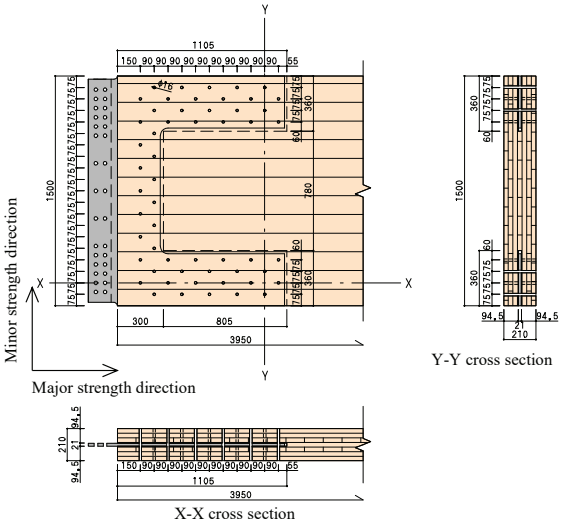

Figure 3: *Test piece for semi-rigid beam end joint full-size in-plane bending test*
(Dimensions are machined CLT dimensions.)

Table 1: *CLT specifications*

Specimen	Density [kg/m^3]	M.C. [%]
C1-F	414	10.4
C2-F	408	10.8
C3-F	424	10.8
Ave.	415	10.7

Table 2: *Mechanical properties of steel used in the tests*

Material	σ_y [N/mm^2]	σ_{max} [N/mm^2]	Yield strain [μ]
Driftpin	326 (0.9%)	459 (0.3%)	-
Steel plate	297 (1.2%)	429 (0.5%)	1434 (0.6%)

* Figures in parentheses are standard deviation values.

2.3 TEST METHOD

Figure 4 shows an overview of the test setup. The test piece was set up by rotating the semi-rigid beam by 90°, clamping the lower end to the test bed with a bracket jig, and applying a force at the point assumed to be the center of the span (the reflexion point of the anti-symmetric bending moment attributable to the seismic force). The force was applied by pushing and pulling the side of the semi-rigid beam using a bearing plate attached to an actuator. To keep the bearing plate from becoming embedded in the timber, we secured steel plates ($t \times H$ = 12 × 225) of identical thickness as the specimen on both sides of the test piece using 60 screws with a diameter of

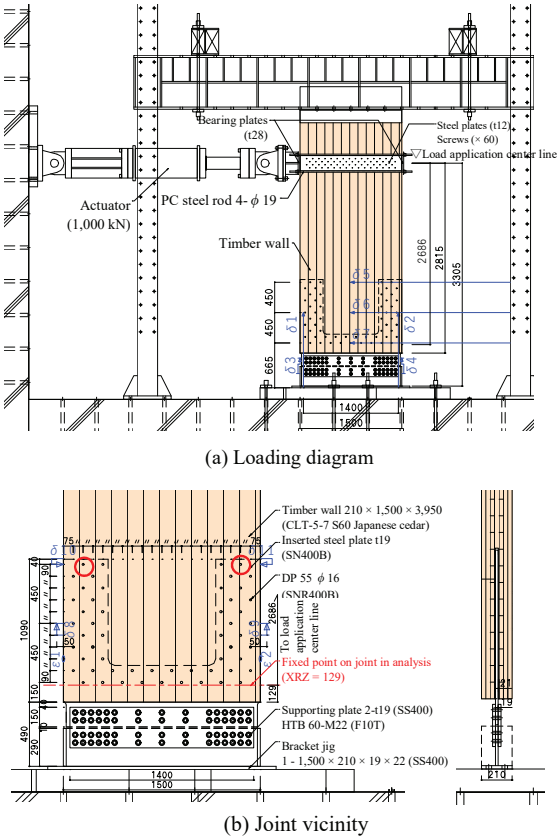

(a) Loading diagram

(b) Joint vicinity

Figure 4: *Overview of vertical wall end joint full-size in -plane bending test*

https://doi.org/10.52202/069179-0433

8 mm and length of 90 mm. We applied the loading by rotating the joint by 1/600, 1/450, 1/300, 1/200, 1/150, 1/100, 1/75, and 1/50 rad three times in succession in the positive and negative directions, and then by 1/30 rad once in the positive and negative directions. We then applied this same loading until the joint had turned by 1/15 rad in the positive direction or until the load declined to 0.8 times of the maximum load. We used Equation (1) to calculate the angular rotation of the joint from the displacement.

$$\theta = \frac{(\delta_2 - \delta_4) - (\delta_1 - \delta_3)}{1{,}400} \quad (1)$$

Here, δ_1 and δ_2 are the displacements (absolute vertical displacement for the CLT) for the 1st and 2nd displacement meters, while δ_3 and δ_4 are the displacements (relative vertical displacement for the CLT and bracket jig) for the 3rd and 4th displacement meters (see Figure 4 (a)). Moment M at the joint is obtained by multiplying the shear force Q measured by the load cell inside the actuator connected to the jack by the distance 2.686 m from the load application point to the fixed point on the joint in the analysis (129 mm from the CLT end; refer to Section 4.4.2 for the definition of the fixed point on the joint in the analysis). Strain gauges (ε1 and ε2) were also attached to the sides of the U-shaped root of the inserted steel plate.

2.4 TEST RESULTS

Figure 5 shows the relationship between the joint moment and rotation angle for all three test pieces. Table 3 lists the characteristic values obtained from the tests. Here, we calculated rotational stiffness K_θ as the mean secant stiffness at the first peak on the positive and negative sides for a control deformation angle of 1/300 rad. We calculated the yield strength of the drift pin joint by setting the mean value of the positive and negative loads as drift pin joint yield strength ${}_{DP}M_y$ for the yield moment of the joint at the point at which the individual drift pin joint on which the greatest stress acts reaches the mean yield point displacement value of 2.65 mm discussed in Section 3. Here, based on the analysis in Section 4, the individual drift pin joint subject to the most severe stress was determined to be the drift pin circled in Figure 4 (b). The corresponding displacement δ_{FDP} was obtained using Equation (2).

$$\delta_{FDP} = \frac{1}{2}\left(\sqrt{\left(\frac{600}{800}\cdot\delta_8\right)^2 + {\delta_{10}}^2} + \sqrt{\left(\frac{600}{800}\cdot\delta_9\right)^2 + {\delta_{11}}^2}\right) \quad (2)$$

Here, δ_8 and δ_9 are the displacements (relative vertical displacement for the CLT and inserted steel plate) for the 8th and 9th displacement meters (see Figure 4 (b)), while δ_{10} and δ_{11} are the displacements (relative lateral displacement for the CLT and inserted steel plate) for the 10th and 11th displacement meters (see Figure 4 (b)).

We calculated the yield strength of the inserted steel plate by setting the mean value of the positive and negative loads as the inserted steel plate yield strength ${}_{PL}My$ for the joint moment at the point at which the strain gauges (ε1 and ε2) mounted on the root of the U-shape of the inserted steel plate reach the tensile yield strain of 1,434 μ (see Table 2) for the inserted steel plate.

We calculated ultimate strength as the mean of the positive and negative loads for moment M_u for which the area of the trapezoid for the elastic perfectly plastic model in which the moment is M_u with the rotational stiffness as the primary gradient within the range up to 1/50 rad is equivalent to the area enclosed by the experimental joint moment and joint rotation angle plot and the X axis.

Behavior was virtually identical for all three test pieces up to a joint rotation angle of 1/30 rad, with none exhibiting significant failure. When the C3-F test piece was pulled beyond 1/30 rad, group shear failure occurred at the drift pin joint under tension at around 1/20 rad. The load dropped to approximately 60%, accompanied by a breaking sound, at which point we stopped the test. The C1-F and C2-F test pieces reached 1/15 rad with no significant reductions in load or group shear failure; we stopped the tests at this point. Figure 5 shows that the drift pin joint yield (${}_{DP}M_y$) and inserted steel plate yield (${}_{PL}M_y$) occurred almost simultaneously.

Figure 6 shows the condition of test piece C1-F after disassembly. Each drift pin is deformed at one or three hinge points along its length. The deformation of the drift pin is more severe in the area framed in red in Figure 6 (a-1) and less severe in the area framed in blue, clearly indicating that the extent of the deformation varies with location. This appears to be because the magnitude of the stress occurring in each drift pin differs with distance from

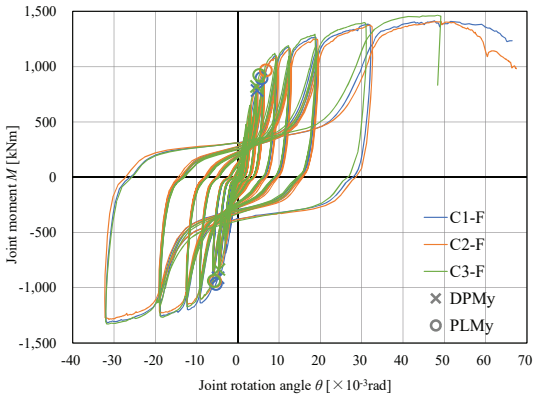

Figure 5: *Relationship between joint moment and rotation*

Table 3: *List of characteristic values obtained from tests*

Test piece	Rotational stiffness K_θ [kNm/rad]	Joint fixed point x_{RZ} [mm]	Drift pin joint yield strength ${}_{DP}M_y$ [kNm]	Steel plate yield strength ${}_{PL}M_y$ [kNm]	Maximum strength M_{max} [kNm]	Ultimate strength M_u [kNm]	
			${}_{DP}\theta_y$ [×10^{-3}rad]	${}_{PL}\theta_y$ [×10^{-3}rad]	θ_{max} [×10^{-3}rad]	θ_v [×10^{-3}rad]	θ_u [×10^{-3}rad]
C1-F	201,620	107	847	930	1,411	1,127	
			4.7	5.5	47.7	5.7	20.0
C2-F	204,578	136	829	953	1,407	1,103	
			4.5	6.1	49.3	5.3	20.0
C3-F	204,529	130	880	932	1,463	1,125	
			5.0	5.5	48.4	5.5	20.0
Ave.	203,576	124	852	938	1427	1119	
			4.7	5.7	48.5	5.5	20.0

https://doi.org/10.52202/069179-0433

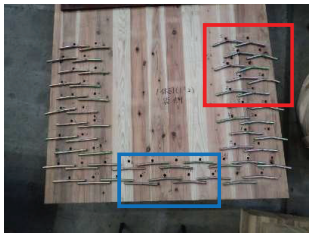

(a-1) Drift pins after disassembly

(a-2) Enlarged view of area framed in red

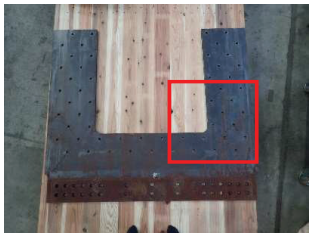

(b-1) Inserted steel plate after disassembly

(b-2) Enlarged view of area framed in red

Figure 6: *Condition of vertical wall end joint full-size in-plane bending test piece after disassembly*

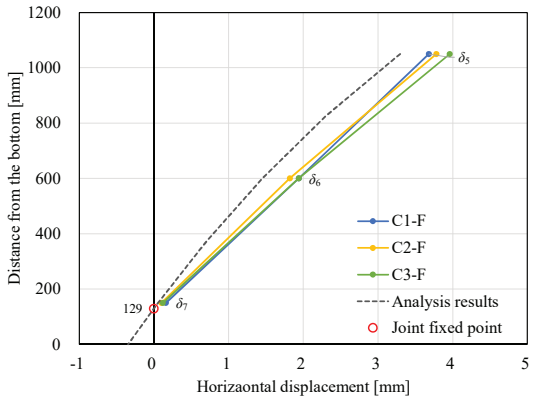

Figure 7: *Test piece horizontal displacement and fixed point*

the center of rotation of the joint. The inserted steel plate is deformed in the direction of the stress acting on the drift pin joint. The root area of the U-shape exhibits delamination of the blackened layer, demonstrating that residual deformation starts at the root area. In conjunction with the state of the test piece, this led us to conclude that the inserted steel plate had yielded at the drift pin joint and the root area of the U-shape.

Figure 7 shows the horizontal displacement (δ_5 to δ_7 in Figure 4 (a)) of the test piece at the positive initial peak in the 1/300 rad cycle. The horizontal axis represents lateral displacement, while the vertical axis represents the distance from the semi-rigid beam end. The fixed point of the joint indicates the distance from the CLT end at which the length of the section is 0 (the horizontal displacement is 0) when a regression line is plotted from the horizontal displacement for each test piece at the corresponding peak. Section 4.4.2 provides more information on the joint fixed point.

3 INDIVIDUAL JOINT TENSILE TEST

3.1 TEST AIMS

With this construction method, drift pins joined to the CLT in the inserted steel plate configuration provide bending resistance, which ensures the specified strength, rigidity, and deformability. A thorough understanding of the performance of the drift pin joint is required to predict the actual rigidity and strength of the joint. At the same time, it is not possible to use the same equations to calculate rigidity [1] and strength [2], as CLT features a laminar configuration with mixed and perpendicular fiber directions. Since the angle θ between the direction of the stress from the drift pin and the direction of the strong axis of the CLT varies depending on the position of the drift pin, it is necessary to identify the effects due to θ.

Thus, we performed tensile tests on individual drift pin joints to confirm individual drift pin joint performance and the effects due to θ.

3.2 TEST PIECE OVERVIEW

The test pieces were manufactured by cutting out pieces of CLT measuring 300 mm in width for each of the four angles, as shown in Figure 8. The CLT used the same parent board as used for the full-size test described in Section 2 (see Table 1 for specifications). The test pieces are referred to as "Cn-Eθ," with "n" indicating parent board number (1, 2, or 3) and "θ" indicating the angle of the applied load with respect to the strong axis of the CLT (0, 30, 60, or 90). The inserted steel plate was made of SN400B, and the drift pins were made of SNR400B. We used two drift pins of each. Table 4 presents the mechanical properties of the drift pins and inserted steel plates. We prepared three test pieces for each of the four angles, with one piece cut out from each parent board. As in Section 2, the holes in the CLT had a clearance of 0 mm with respect to the drift pins, while the holes in the inserted steel plates had a clearance of + 1 mm. The slit in the CLT had a clearance of + 2 mm with respect to the inserted steel plate.

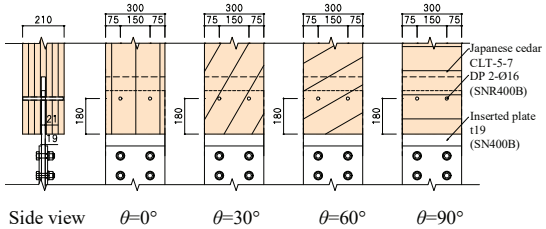

Figure 8: *Overview of individual joint tensile test pieces*

Table 4: *Mechanical properties of steel used in tests*

Material	σ_y [N/mm^2]	σ_{max} [N/mm^2]
Driftpin	326 (0.9%)	459 (0.3%)
Steel plate	312 (2.0%)	431 (0.4%)

* Figures in parentheses are standard deviation values.

https://doi.org/10.52202/069179-0433

3.3 TEST METHOD

Figure 9 shows the loading configuration. Loads were applied using 1,000 kN center hole jacks for tensioning and compressing. Axial forces were measured using pressure transducers connected to each jack. We measured the relative displacement between the inserted steel plate and the CLT at two points (on the front and back) and used the mean value as the joint displacement. We performed positive and negative loading three times and treated tensile loading as positive loading. These loads were applied by repeatedly applying displacements of $\delta pt \times 1/2$, 1, 2, 4, 6, 8, 12, and 16, based on the yield displacement of δpt = 1.55 mm in the preliminary test done at θ = 0°, until the load declined to 0.8 times of the maximum load or until the displacement reached 30 mm.

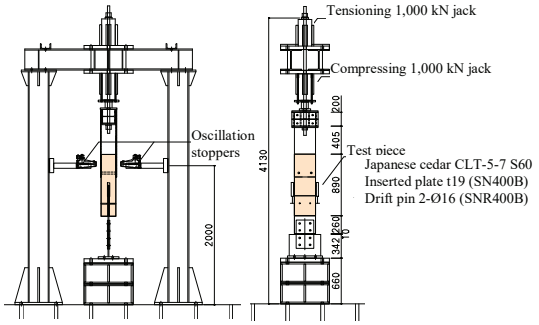

Figure 9: *Individual joint tensile test loading configuration*

3.4 TEST RESULTS

Figure 10 shows the relationship between load per drift pin and deformation for each angle. Table 5 shows the mean characteristic values (θ = 0, 30, 60, and 90 values are mean values for three test pieces; ALL values are mean values for all 12 test pieces) obtained in the tests. We calculated characteristic values such as yield strength and initial stiffness by the method described in reference [3]. The red lines in Figure 10 indicate the mean values for the tri-linear models with test pieces corresponding to each specification. Here, the first breakpoint of the tri-linear model is the point (P_y, δ_y), and the second breakpoint of the tri-linear model is the point (P_{max}, δ_{max}). After testing, we removed the drift pins, assigning those showing zero bending points to Yield Mode I, those with one bending point to Yield Mode III, and those with three bending points to Yield Mode IV. Figure 11 shows some of the disassembled test pieces.

The load-displacement relationship shown in Figure 10 confirmed that stiffness for all test pieces begins to decline at a relative displacement of approximately 2 mm. When the test pieces were disassembled, the drift pins demonstrated behavior corresponding to Yield Mode III or IV. This suggests that drift pin yield occurred and that bearing yield occurred in timber parts in contact with the drift pins. Ultimately, the load declined with each repetition for 16 × δ_{pt} cycles. Examination of the drift pins after disassembly showed that many had failed from the area at which they were in contact with the inserted steel plate near the center. We estimate that fatigue fracture occurred at 16 × δ_{pt} cycles.

When we compared the direction θ of the stress acting from the drift pin, we found no obvious differences due to θ for initial stiffness or joint yield strength. Based on this, we conclude that the effects on individual drift pin performance due to the direction θ of the stress acting from the drift pin are negligible.

Table 5: *Characteristic values obtained from tests*

Actual angle [°]	Yield strength P_y [kN] / Yield displacement δ_y [mm]	Maximun strength P_{max} [kN] / Displacement at Pmax δ_{max} [mm]	Initial stiffness K_1 [kN/mm]	Secondary stiffness K_2 [kN/mm]	Mode
0	31.6 / 2.79	47.0 / 24.3	11.6	0.72	IV,IV,IV
30	29.4 / 3.05	44.9 / 22.7	10.0	0.79	IV,IV,IV
60	31.4 / 2.21	46.3 / 24.8	14.4	0.66	IV,IV,IV
90	32.6 / 2.56	45.7 / 24.4	13.3	0.60	III,III,IV
ALL	31.3 / 2.65	46.0 / 24.0	11.8	0.69	-

θ=0° θ=60°

Figure 11: *Condition of joint tensile test pieces after disassembly*

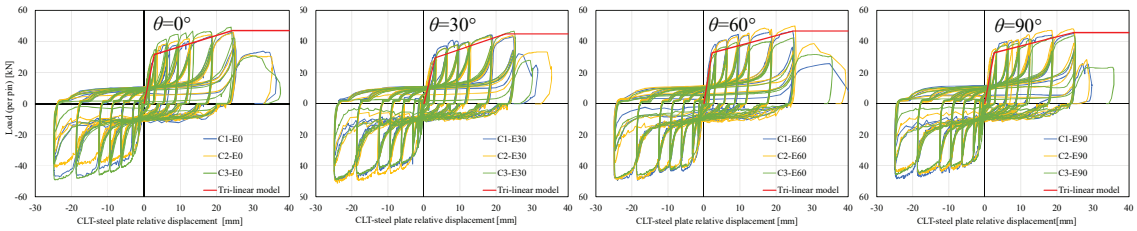

Figure 10: *Individual joint tensile test load displacement relationship*

https://doi.org/10.52202/069179-0433

4 FINITE ELEMENT METHOD ANALYSIS

4.1 ANALYSIS AIMS

We performed our analysis by the finite element method for the semi-rigid beam end joint full-size bending test performed in Section 2. We then compared the analysis results to the test results. Here, we drew on the measurements obtained in the tests described in Section 3 to assess individual drift pin joint and material strength for the inserted steel plate.

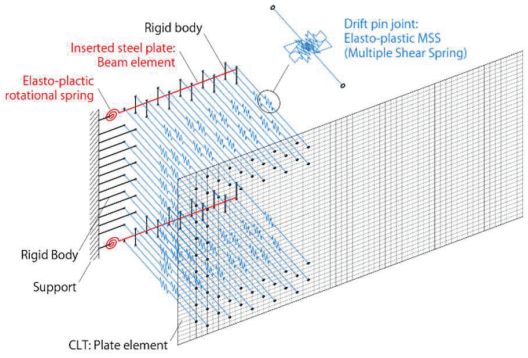

Figure 12: *Overview of analysis model*

Table 6: *Analysis model details*

Element	Element type	Details
CLT	Plate element	t=210mm, E_0=4,285kN/mm^2, E_{90}=1,714N/mm^2, G=0.5kN/mm^2
Drift pin	MSS (n=4)	k_1=5.90kN/mm, p_1=10.52kN k_2=0.342kN/mm, p_2=15.45kN
Inserted steel plate	Beam element	B×D = 19mm×340mm Elasto-plastic spring for root area (See Figure 13.)

* E_o : Young's modulus in strong axis direction,
E_{90} : Young's modulus in weak axis direction
G : Elastic shear modulus
k_1,k_2: Stiffness of each shear spring
p_1,p_2: Strength of each shear spring

4.2 ANALYSIS MODEL

Table 6 lists the details of the analysis model. Figure 12 provides an overview of the model. CLT stiffness is specified as described in reference [4]. We modeled the inserted steel plate individual drift pin joint as a tri-linear model using a multiple shear spring (MSS, with number of partitions n = 4). We calculated individual shear spring stiffness value k_1 and k_2 and yield load p_1 and p_2 by applying the following equations, as in reference [5].

$$k_1 = {K_1}\Big/{\sum_{i=1}^{n} \sin^2 \frac{1}{n}\pi} \quad (3)$$

$$k_2 = {K_2}\Big/{\sum_{i=1}^{n} \sin^2 \frac{1}{n}\pi} \quad (4)$$

$$p_1 = {P_y}\Big/{\sum_{i=0}^{n-1} \sin \frac{1}{n}\pi} \quad (5)$$

$$p_2 = {P_{max}}\Big/{\sum_{i=0}^{n-1} \sin \frac{1}{n}\pi} \quad (6)$$

Here, k_1 is the initial stiffness of each shear spring [kN/mm], p_1 is the first yield load for each shear spring [kN], k_2 is the secondary stiffness of each shear spring [kN/mm], p_2 is the second yield load for each shear spring [kN], K_1 is the initial stiffness of the individual joint [kN/mm], K_2 is the secondary stiffness of the individual joint [kN/mm], P_y is the yield strength of the individual joint [kN], and P_{max} is the maximum strength of the individual joint [kN]. Each Characteristic value of the individual joint are treated as independent of angle based on the test results described in Section 3, in which we observed no obvious differences due to angle for either. Thus, we used the mean values of the test results for all 12 test pieces (see Table 5 for values).

We modeled the inserted steel plate root area as a rotational spring with tri-linear restoring force properties, as shown in Figure 13. The initial stiffness was set to K_0 = 135,912 kNm/rad, derived from the elastic analysis of the U-shaped steel plate. With the rotational spring, we replaced the skeleton curve obtained from the results of equations (7) to (13) while reducing the stiffness by the ratio of the cross-sectional moment of inertia of the residual elastic region to the cross-sectional moment of inertia of the entire cross section with a tri-linear model.

$$M_y = Z \cdot \sigma_y \quad (7)$$

$$M_p = Z_p \cdot \sigma_y \quad (8)$$

$$M_i = M_y + (M_p - M_y)i/m \quad (9)$$

$$x_i = \sqrt{\frac{3D^2}{4} - \frac{3M_i}{B\sigma_y}} \quad (10)$$

$$I_i = \frac{B(2x_i)^3}{12} \quad (11)$$

$$K_i = I_i / I_0 \, K_0 \quad (12)$$

$$\theta_i = \theta_{i-1} + \frac{(M_p - M_y)/m}{(K_i + K_{i-1})/2} \quad (13)$$

Here, M_y is the yield moment [kNm]; Z is the section modulus [mm^3]; σ_y is the inserted steel plate yield stress (= 297) [N/mm^2]; M_p is the fully plastic moment [kNm]; Z_p is the plastic section modulus [mm^3]; i is the number of steps; m is the number of divisions (= 10); M_i is the bending moment for step i [kNm]; x_i is the non-plasticized part thickness for step i [mm]; D is the steel plate thickness (= 340) [mm]; B is the steel plate width (= 19) [mm]; I_i is the cross-sectional moment of inertia for step i [mm^4]; K_i is the rotational stiffness for step i [kNm/rad]; and θ_i is the rotation angle for step i [rad].

The first break point with the tri-linear model occurs when the yield moment M_y is reached. The second break point occurs when the fully plastic moment M_p is reached. These were determined so that Area 1 and Area 2 in Figure 13 are identical. The calculations here for M_y and M_p assume the inserted steel plate yield stress of 297 kN/mm^2 (see Table 2) used in Section 2 for the inserted steel plate yield stress.

https://doi.org/10.52202/069179-0433

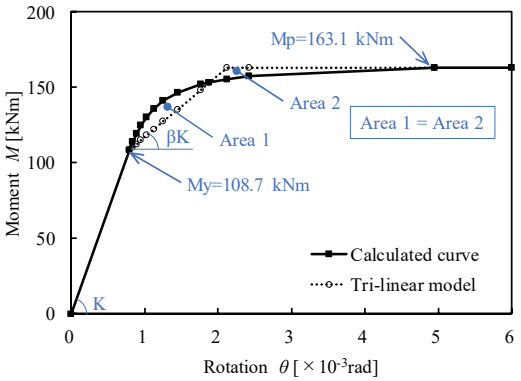

Figure 13: *Rotational spring of inserted steel plate root area*

4.3 ANALYSIS CONDITIONS

The model set was subjected to static incremental loading analysis. Figure 14 shows the analysis conditions. Incremental loading analysis was performed by positioning the load 2,815 mm from the end of the CLT in the same way as in the full-size tests, with the 41 nodes at that position connected to rigid beam elements. A nodal load was applied to the uppermost node.

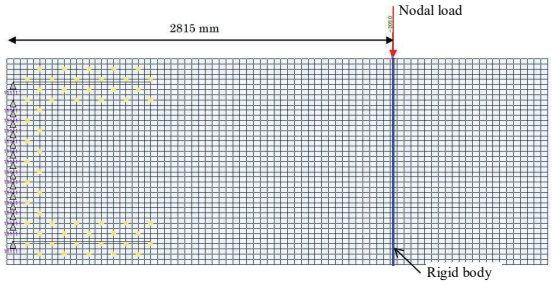

Figure 14: *Analysis conditions*

4.4 ANALYSIS RESULTS

4.4.1 Moment-rotation angle relationship

Figure 15 shows the relationship between moment and rotation angle for the joint. Joint moment M is defined as the value obtained by multiplying the shear force applied to the model by the moment arm length (described later) of 2.686 m. The solid lines indicate the results for the three test pieces. The dashed lines indicate incremental analysis results. The "×" symbols (M = 785 kNm, $\theta = 3.91 \times 10^{-3}$ rad) on the dashed line indicate the point at which the displacement of the first drift pin reaches the yield displacement δ_y 2.65 mm of the individual joint in the incremental analysis. The joint load moment at this point is defined as the yield moment ${}_{DP}M_y$ of the drift pin joint obtained from the analysis. The "○" symbols (M = 917 kNm, $\theta = 4.99 \times 10^{-3}$ rad) indicate the point at which bending yield occurs at the root of the inserted steel plate in the incremental analysis (when M_y in Figure 13 is reached). The joint load moment at this point is defined as the yield moment ${}_{PL}M_y$ of the drift pin joint obtained from the analysis. Figure 15 shows that the drift pin yield and inserted steel plate bending yield in the analysis relatively near-simultaneously.

Table 7 compares the mean test results and analysis results for the rotationnal stiffness, yield strength, and ultimate strength of the joint. Ultimate strength M_u in the analysis results is defined as the joint moment when a bi-linear curve is drawn so that the initial gradient is the rotational stiffness and the area is equivalent to the joint moment-rotational angle relationship in the range up to 1/50 rad.

From Figure 15, the finite element method analysis was able to track the experimental results with good accuracy. The load increase after yielding can be reproduced by inputting the spring of the drift pin joint and the inserted steel plate at root area of the U-shaped part with a tri-linear type. The difference between the analysis results and the experimental results is large in the range of after 1/50 rad, but this is considered to be because the decrease in strength after reaching the maximum strength of each element was not reproduced in the analysis.

4.4.2 Joint fixed point position

This paper defines as the joint fixed point the point on a semi-rigid beam joint at which no displacement occurs when a load results in rotational deformation. The distance from the point at which the force is applied to the fixed point of the joint is used as the moment arm length for the calculation of the joint moment.

Figure 7 shows the 1/300 rad cycle positive peak for the semi-rigid beam end joint full-size in-plane bending test, together with the analysis results for the same load conditions. The analysis results at this point are within the elastic range. Figure 7 confirms that the joint fixed point generally coincides with the test results. Based on these results, we defined the y-intercept (= 129 mm) of the analysis results (dashed line) as the joint fixed point position. Based on the dimensional relationship shown in Figure 4, we calculated the moment arm length to be 2,686 mm (= 2,815 mm - 129 mm).

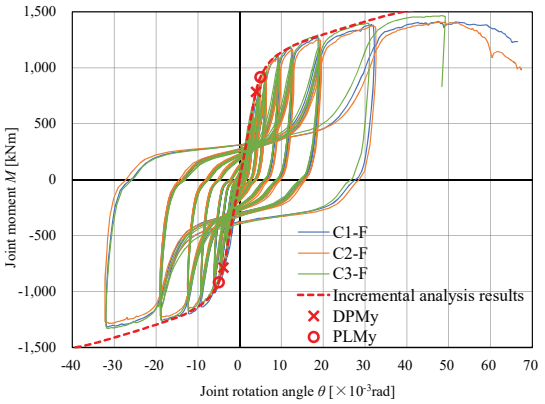

Figure 15: *Joint moment-rotation angle relationship (Comparison of test results and analysis results)*

Table 7: *Comparison of test data and analysis data*

Test Ppiece	Rotational stiffness K_θ [kNm/rad]	Driftpin joint yield strength ${}_{DP}M_y$ [kNm]	Steel plate yield strength ${}_{PL}M_y$ [kNm]	Ultimate strength M_u [kNm]
Test data (mean of 3 values)	203,576	852	938	1,119
Analysis data	202,716	785	917	1,168
Analysis data/Test data	1.00	0.92	0.98	1.04

https://doi.org/10.52202/069179-0433

5 CONCLUSIONS

We carried out full-size in-plane bending tests on the end joint, and finite element method analysis to verify the performance of joints on semi-rigid timber beams using CLT. Our findings are presented below.

- Full-size in-plane bending tests on the end joint of semi-rigid timber beams using CLT demonstrated the capacity to achieve the specified strength and deformability.
- The bending yield of individual drift pin joints and the bending yield of the U-shaped inserted steel plate root area may improve the deformability of semi-rigid timber beam joints.
- Both individual joint initial stiffness and joint strength had minimal dependence on angle, given the specifications used in the individual joint tensile tests.
- The results confirm that an analysis model based on the finite element method can accurately evaluate the experimental values.
- The position of the point at which displacement does not occur (joint fixed point) was determined from the analysis results. The results for the joint fixed point were generally consistent with test results.

ACKNOWLEDGEMENTS

This study was carried out using materials kindly provided by Meiken Lamwood Corp. We are grateful for the support of all those involved.

REFERENCES

[1] Kuenzi EW : Theoretical design of a nailed or bolted joint under lateral load, USDA, No.D1951, March 1955

[2] Johansen K. W.: Theory of timber connections, Int. Assoc. Bridge and Struct. Eng 9 : pp.249-262, 1949

[3] Japan 2×4 Home Builders Association : Structural Calculation Guideline for Platform Frame Wall Construction, 2007.

[4] Japan housing and Wood Technology Center : Design and Construction Manual for Timber Structures using Cross Laminated Timber (CLT), 2016.

[5] Architectural Institute of Japan : Recommendation for the Design of Seismically Isolated Buildings, 2013.